Supplemental Information

Functional Organization of Human Sensorimotor Cortex for Speech Articulation

Kristofer E. Bouchard[1,2], Nima Mesgarani[1,2], Keith Johnson[3], and Edward F. Chang[1,2,4]

1. Departments of Neurological Surgery and Physiology, University of California, San Francisco
2. Center for Integrative Neuroscience, University of California, San Francisco
3. Department of Linguistics, University of California, Berkeley
4. UCSF Epilepsy Center, University of California, San Francisco

Supplementary Figure 1

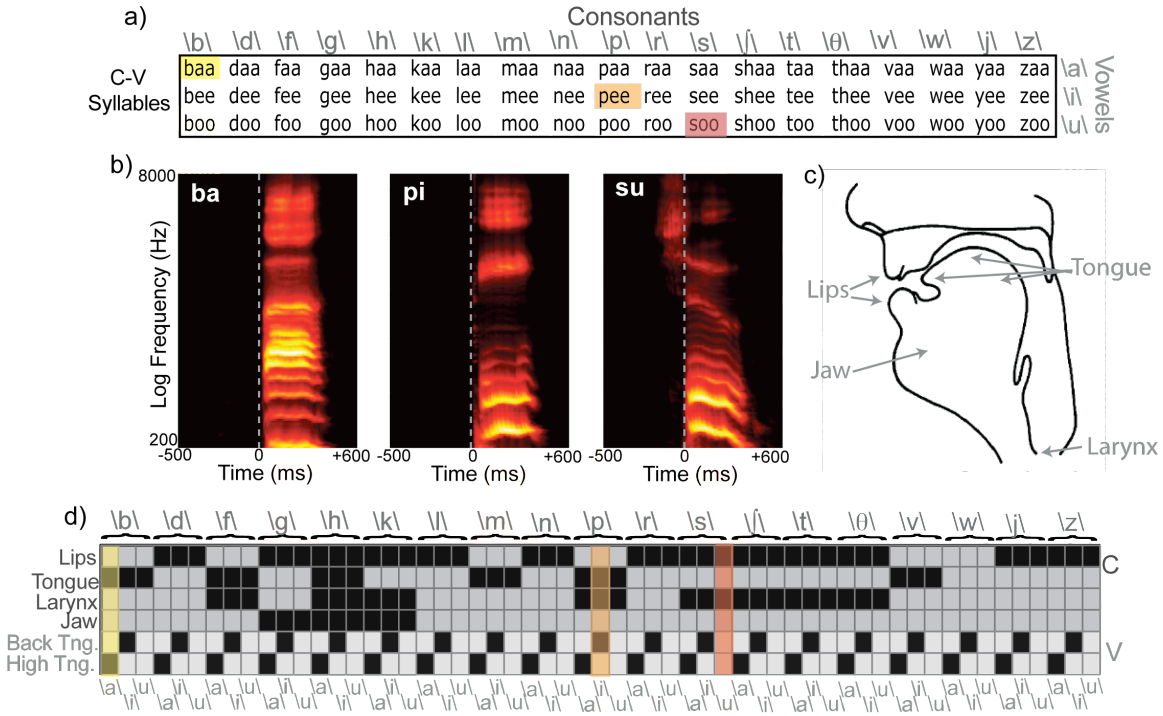

Supplementary Figure 1. Task Design and Behavioral Analysis
a) Consonant-Vowel Matrix and IPA phonetic symbols. Neurosurgical patients read aloud from a list of consonant-vowel syllables (CVs), consisting of 19 consonants followed by one of three vowels (/a/, /u/, or /i/). The IPA notations for the consonant and vowel are displayed as column and row headings, respectively, with entries in the matrix specifying the American English pronunciation.

b) Cochlear spectrograms for three syllables aligned at the acoustic onset of the consonant-to-vowel transition. To analyze the consonant and vowel phases of our CVs from a common temporal reference point, all behavioral and electrophysiological data are aligned at the acoustic onset of the consonant-to-vowel transition (t = 0). The acoustic onset of the C-V transition is displayed as the dashed grey line overlaid on the cochlear spectrograms for three syllables with temporally distinct consonants (/b/, /p/, /s/).

c) Diagram of the vocal tract with respect to the four major articulator organs analyzed in this study: tongue, lips, jaw, and larynx

d) Articulator State Matrix. Each CV is described by a six element binary vector indicating its articulatory organ engagement. Each vector consisted of four variables corresponding to the four main upper-vocal tract articulatory organs (Lips, Tongue, Larynx, Jaw) for consonants and two variables describing the tongue configuration for vowels (Back Tongue and High Tongue). Furthermore, they constitute a linearly independent basis set with which to describe the CVs in our dataset. This linear independence is preferred given the linear methods used for articulatory analysis (general linear models and partial correlation analysis).

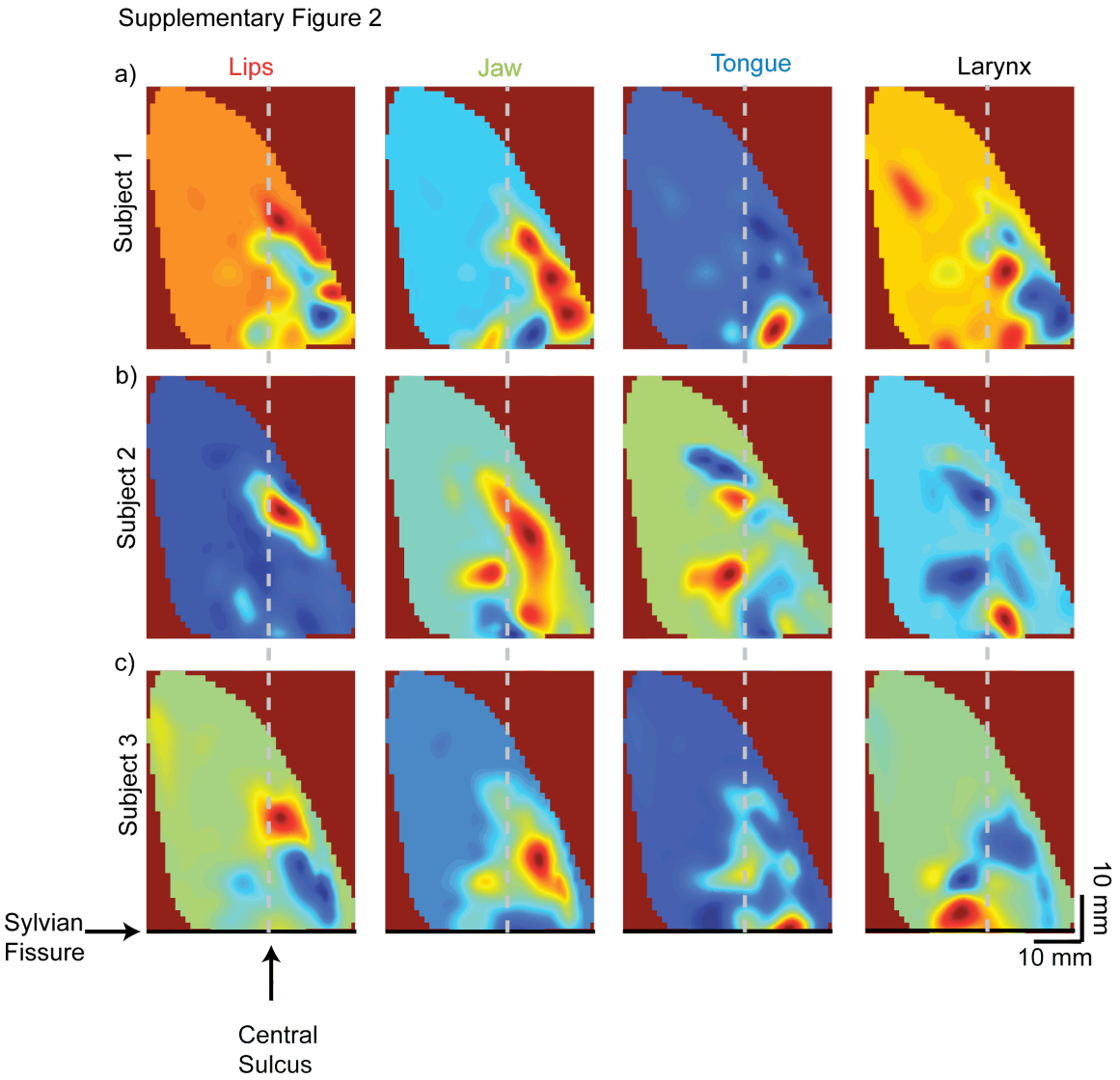

Supplementary Figure 2. Spatial topographic organization of articulator representations in vSMC for individual subjects.

a-c) Topographic organization of articulator weightings for each subject. The optimal weighting assigned to each articulator (Lips, Jaw, Tongue, and Larynx) by the general linear model analysis presented as a heat map in Cartesian space, defined by distance from Central Sulcus (ordinate) and Sylvian Fissure (azimuth). Dashed vertical gray line corresponds to the Central Sulcus.

Supplementary Figure 3

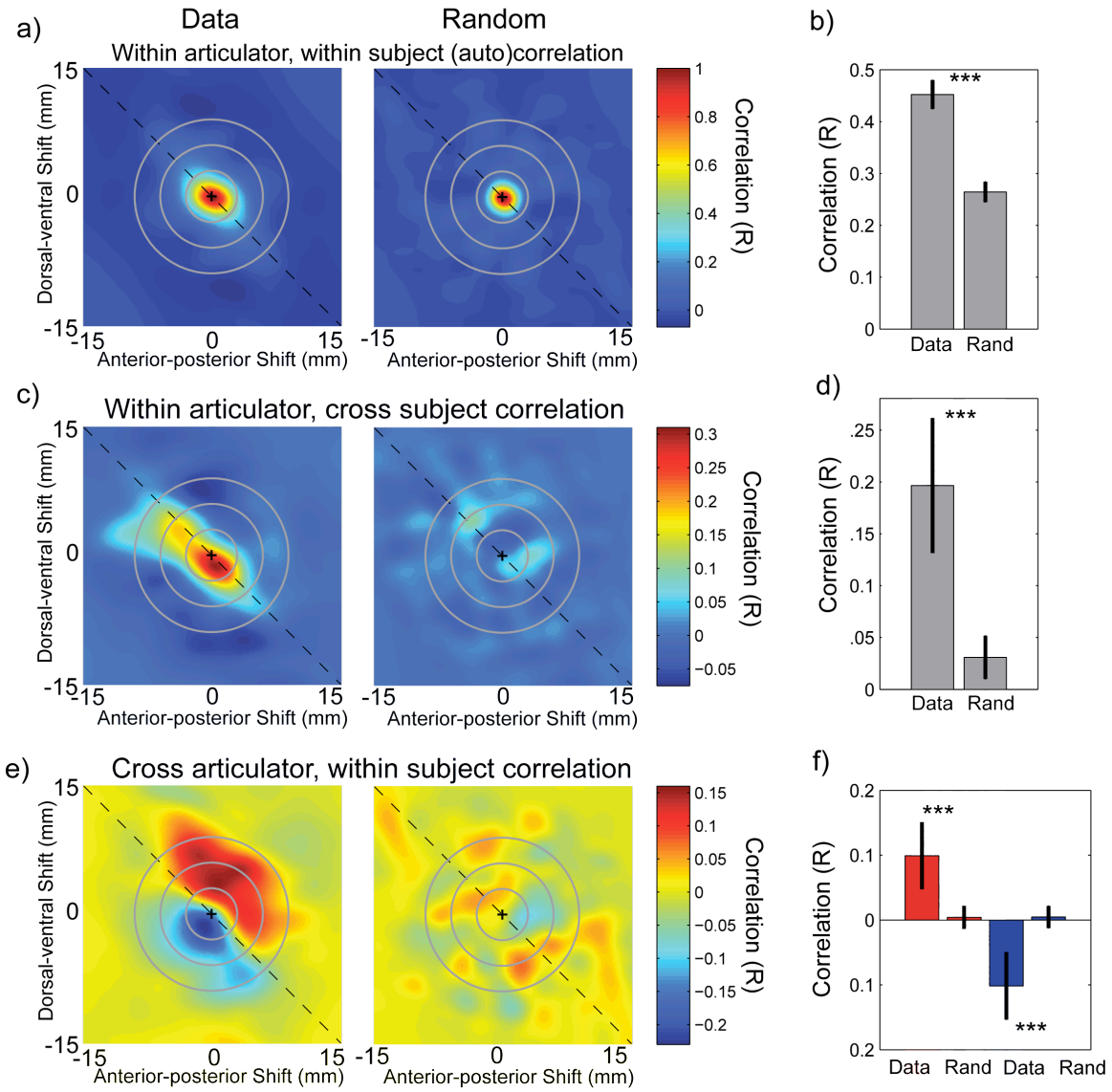

Supplementary Figure 3. Spatial structure of articulator representations is statistically similar across subjects

We quantitatively analyzed the spatial organization of articulator representations using a two-dimensional cross-correlation analysis. This quantifies the similarity of spatial structure of two matrices as they are 'slid' over each other at different spatial shifts in the x-direction (anterior-posterior direction, abscissa) and y-direction (dorsal-ventral direction, ordinate). Large positive values (red) indicates large correlations, corresponding to similar spatial organization at a given [x,y] shift. Generally speaking, two-dimensional cross-correlation analysis is capable of revealing important spatial characteristics such as: spatial isolation/distribution, spatial anisotropies, spatial location similarity and spatial sequences. To gauge the statistical significance of the observed cross-correlation values, we created a null dataset by randomly shuffling (1000 times) the location of electrodes with in each subject. Other than the randomization, observed and null datasets are processed and analyzed identically. In each plot, the cross

mark (+) in the center corresponds to the point of no shift in either direction ([0, 0]). Values above the dashed black line correspond to dorsal-posterior shifts. Grey circles correspond to concentric shifts of 3, 6 and 9 mm.

(a-b) Spatial structure of individual articulator representations.
We examined the spatial structure of individual articulator representations by taking the spatial autocorrelation of each map in each subject (S1-S3). If individual electrodes for specific articulators are randomly organized with respect to one another, we expect to see a single large peak at zero shift ([0,0]) that falls off symmetrically with (x,y) shifts and has a radius of ~2 mm (size of smoothing kernel)(a, Random). We found that the representations of individual articulators were spatially well isolated in each subject (large single peak at [0,0]), but tended to be spatially clustered (correlation has greater spatial extent than random scattering). There also appeared to be a relatively consistent anisotropy along the anterior-dorsal/posterior-ventral axes (dashed line). These features are summarized in the left plot in (a, Data) by averaging the individual articulator x subject spatial autocorrelation functions. For comparison, an example of the average autocorrelation function derived from a single random permutation of the spatial location of each subject's electrodes is presented on the right (a, Random).
(b) We quantified the difference between the observed and random autocorrelations by averaging the values with in a 3 mm radius (innermost ring) for each comparison. The correlation values for the data (0.45 ± 0.03, mean ± s.e., 3 subjects x 4 articulators, n = 12) were significantly greater than for the randomized data (0.26 ± 0.02, mean ± s.d., 1000 randomizations for each subject; $P < 10^{-3}$). Therefore, electrodes with similar representations are spatially closer to one-another than expected by chance.

(c-d) Spatial location of individual articulator representations is statistically similar across subjects.
We examined the across-subject similarity of spatial location for individual articulator representations by taking the spatial cross-correlation of each articulators map across pair-wise subject comparisons (S1-S2, S2-S3, and S1-S3).
If the representation of an individual articulator occupies a similar spatial location across subjects, we expect to see large correlations centered at [0,0] and that fall off with distance. This analysis revealed that the representations of individual articulators were in similar locations across subjects, as evidence by the large values (red) very near the center of the heat map, corresponding to zero relative shift. The similarity in spatial localization is summarized in (c) by averaging the individual with-in articulator, cross-subject cross-correlations functions, which exhibits a peak near [0,0]. Given the anisotropy described in (a), we expect a similar anisotropy to be seen here. For comparison, an example of the average with-in articulator, cross-subject correlation function derived from a single random permutation of the spatial location of each subject's electrodes is presented on the right (c, Random). (d) We quantified the difference between the observed and random correlations by averaging the values with in a 3 mm radius for individual comparisons. The correlation values for the data (0.195 ± 0.064, mean ± s.e., 3 subjects x 4 articulators, n = 12) were significantly greater than for the randomized data (0.031 ± 0.021, mean ± s.d., $P < 10^{-3}$, 1000 iteration permutation test). Therefore, the representation of individual articulators is more consistently located across subjects than expected by chance.

(e-f) Spatial sequence of articulator representations is statistically observed for each subject
We examined the with-in subject spatial sequence of articulator representations by taking the spatial cross-correlation between spatially adjacent representations (Larynx->Tongue, Tongue->Jaw, Jaw-> Lips), within each subject. Given the anisotropy of individual articulator representations (a), if the dorsal-ventral sequence of articulator representations described in Figure 2 is robust at the single subject

level, then we expect to see a negative-to-positive transition of the correlations about the main diagonal (dashed black line). This analysis revealed that the representations of individual articulators were spatially sequenced along the dorsal-ventral axis, as evidenced by the negative-to-positive transition across the dashed line. The similarity in spatial sequencing is summarized in (e) by averaging the individual cross-articulator, with-in subject cross-correlation functions. The change in sign of the spatial cross-correlation function about the diagonal is the telltale signature of a spatially sequenced organization. For comparison, an example of the average cross-articulator, within-subject correlation function derived from a single random permutation of the spatial location of each subject's electrodes is presented on the right (e, Random). (f) We quantified the difference between the observed and random correlations by averaging the values within the 6 mm semi-circle above and below the diagonal separately for individual comparisons. The correlation values for the above diagonal data were positive (0.099 ± 0.052, mean ± s.e., 3 subjects x 3 cross-articulator comparisons, $n = 9$) and significantly greater than for the randomized data (0.004 ± 0.018, mean ± s.d., 1000 permutations for each subject; $P < 10^{-3}$); in contrast, the correlation values for the below diagonal data were negative (-0.102 ± 0.052, mean ± s.e., $n = 9$) and significantly greater (in magnitude) than for the randomized data (0.005 ± 0.017, mean ± s.d., $P < 10^{-3}$, 1000 permutations for each subject). Therefore, the dorsal-ventral sequence of articulator representations is stronger than expected by chance.

Together, the data and analysis presented in Supplementary Figures 2-3 demonstrate that the representational organization of the articulators in individual subjects is statistically similar. Furthermore, these analyses suggest that the coordinate system used here (anterior-posterior distance relative to the central sulcus and dorsal-ventral distance relative to Sylvian Fissure), is an important organizational reference frame for Rolandic cortex.

Supplementary Figure 4

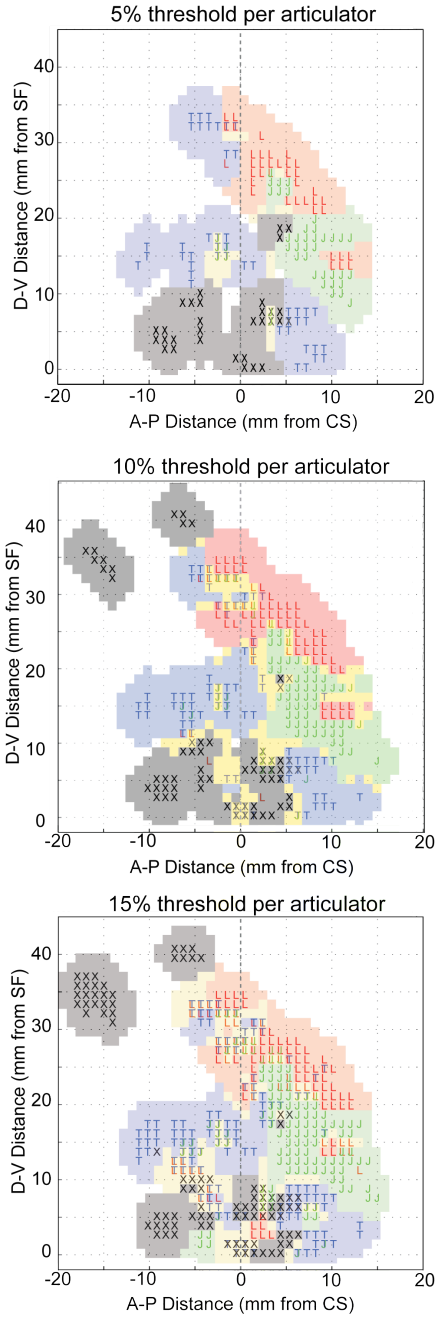

Supplementary Figure 4. Combined articulator maps for different thresholds of individual articulator weights

To provide complementary visualizations of articulator representations presented in Figure 2b, we present articulator maps derived from the k-nearest neighbor classification scheme based off of articulator locations for three different weighting thresholds. a) 5%, b) 10%, c) 15%. As would be expected from the analysis presented in Figure 2, high thresholds resulted in the most delineated articulator maps (5%), and as the threshold for data inclusions is lowered, the maps exhibit more articulator overlap (gold pixels) and became more 'fractured', with different articulator representations being spatially interdigitated.

Supplementary Figure 5

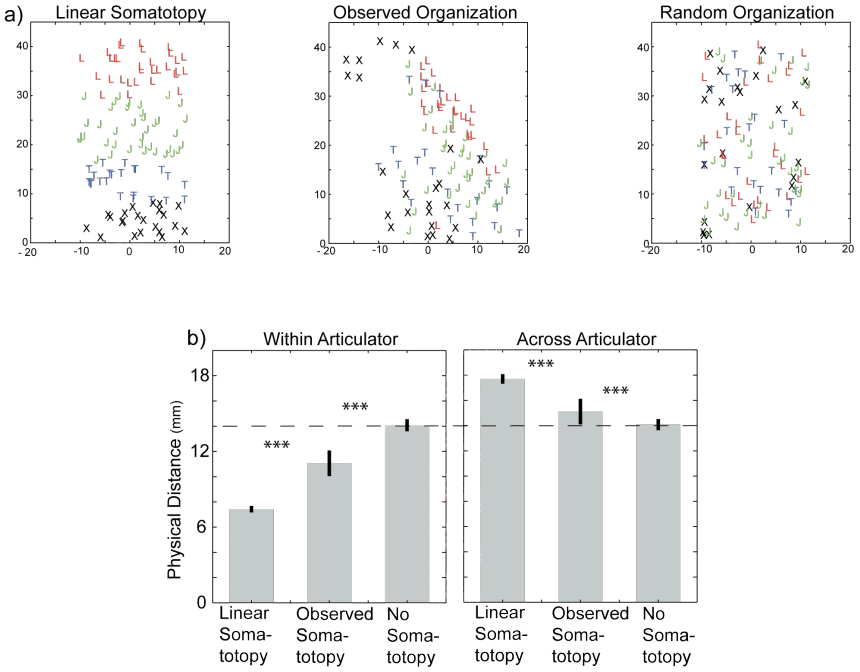

Supplementary Figure 5. Observed articulator organization is neither a perfect linear somatotopy nor a random distribution

To further understand the observed functional organization of articulator representations, we measured the average Euclidean distance (in mm) between electrodes categorized according to their preferred articulator (winner-take-all categorization). We compared the distributions of average intra-articulator distances and cross-articulator distances to predictions from a perfect linear somatotopy and from a completely random distribution (1000 simulated maps each, see Methods). These null models had similar parameters to the observed organization (same number of points per articulator, approximately the same range of spatial values and total area covered) and were used as bounding conditions to set the scale for possible outcomes. The observed map is presented in the middle panel of Supplementary Figure 5a, and is flanked by an example perfect linear somatotopy (left) and an example random scattering (right). (b) Distributions of intra-articulator distances (left) and cross-articulator distances (right) are summarized below. The perfect linear somatotopy minimizes the intra-articulator distances (7.43 ± 0.25 mm, mean ± s.d., 1000 maps) at the expense of maximizing the cross-articulator distances (17.7 ± 0.38 mm, mean ± s.d., 1000 maps); conversely, on average, the random scattering has equal distances with-in and across articulators (14.08 ± 0. 48mm vs. 14.07 ± 0.44mm, mean ± s.d., 1000 maps, dashed grey line). The observed intra-articulator distances (11.06 ± 1.01 mm. mean ± s.e., n = 3188 pair-wise distances) and across articulator distances (15.11 ± 1.01mm, mean ± s.e., n = 4587 pair-wise distances) are both intermediate to these bounding values and are significantly different from both the perfect linear somatotopy and the random scattering ($P > 10^{-3}$). These results suggest that the observed anatomical organization of articulator representations may reflect a weighted balance of simultaneous constraints on intra-articulator and cross-articulator distances. This may support the integration of multi-articulator information by reducing the physical distance between different articulators, perhaps decreasing delays in neuronal transmission.

Supplementary Figure 6

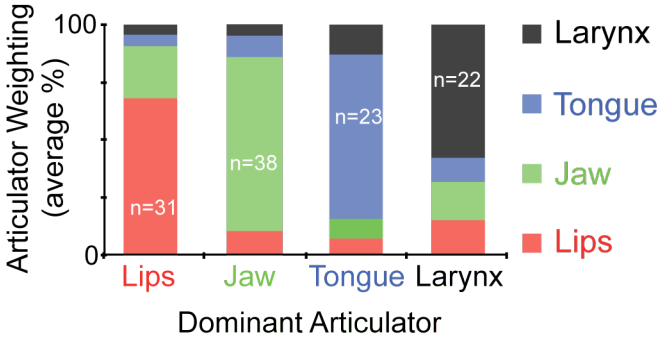

Supplementary Figure 6. Distribution of fractional articulator weightings at individual electrodes We further characterized distributions of articulator weightings at a finer spatial scale by calculating the fractional representation of all articulators at single electrodes. This figure displays the functional distribution of articulator representations at individual electrodes, categorized according to dominant articulator representation. Displays give average articulator weightings as percentage of total. This analysis revealed clear preferred tuning for individual articulators at single electrodes (Fig. 2c, electrodes categorized according to the strongest articulator representation), and also demonstrated that single electrodes had functional representations of multiple articulators.

Supplementary Figure 7

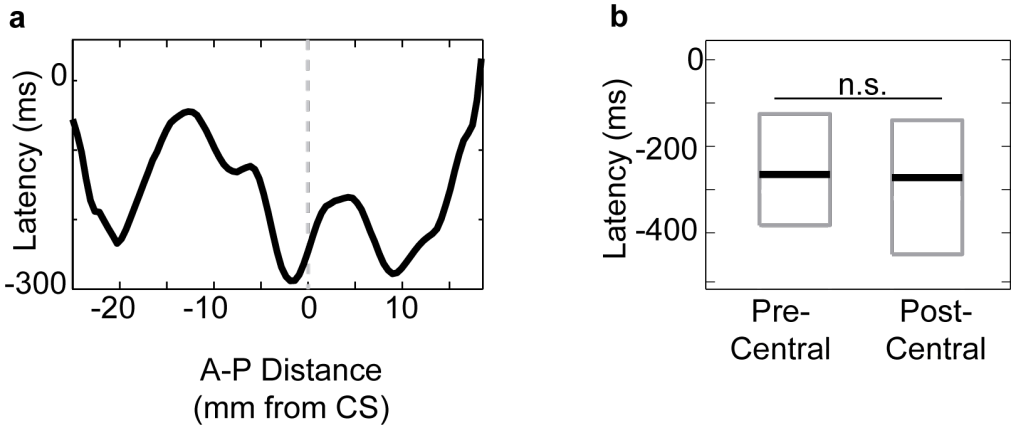

Supplementary Figure 7. Activation latencies are similar between the pre-central gyrus, the post-central gyrus, and across the guenon

We examined whether activation timing differences could dissociated between motor and somatosensory processing. For each electrode, we calculated the onset latency of the coefficient of determination (R^2), which quantifies how well the linear articulator model fit the cortical data. We observed that onset latencies occurred before the CV transition and, contrary to our expectations, we found no significant latency differences in those areas immediately anterior and posterior to the central sulcus (±10 mm), or across the geunon (a-b, $P > 0.4$, Rank-Sum test; n = 71 and n = 67 electrodes respectively, from three subjects). This suggests that cortical activity recorded throughout the vSMC has significant motor components that are difficult to disambiguate from afferent sensory processes.

Supplementary Figure 8

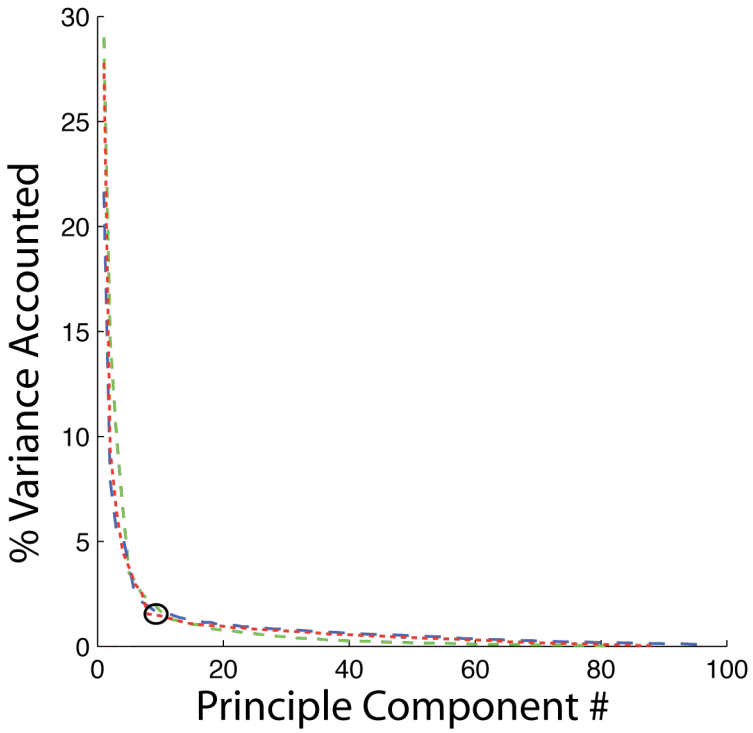

Supplementary Figure 8. Structure of spatial principal components is similar across subjects. Percent variance accounted for by each spatial PC for all three subjects (subjects are in different colors). Across subjects, the amount of accounted for variance decreased sharply over the first nine PC's (black circle) and exhibited a very gradual decline thereafter. This indicates that the first nine PC's correspond to the dimensions that discriminate the CVs. We therefore used the 1st nine PC's as the cortical state-space. The across-subject differences in the decay after nine components can be explained by the different number of electrodes recorded in each subject. Small changes in the number of dimensions did not qualitatively change the results.

Supplementary Figure 9

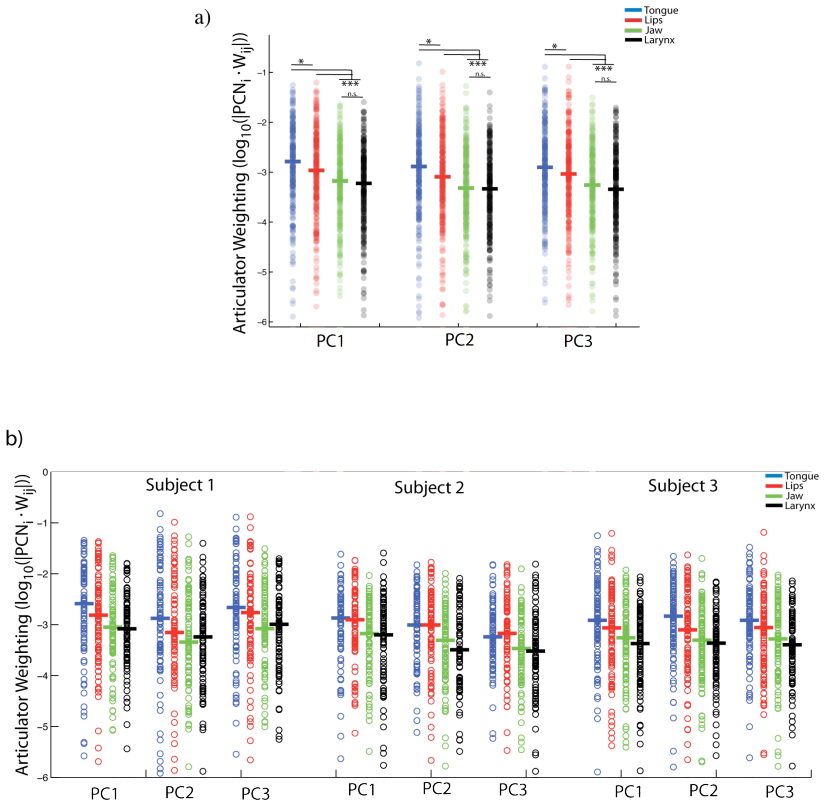

Supplementary Figure 9. Structure of principal components is weighted towards modulations of tongue and lips over larynx and jaw

a) Magnitude of articulator weightings in the 1st three PC's across all subjects (Tongue: blue, Lips: red, Jaw: green, Larynx: black). To understand the contribution of each articulator to the principal components that define the cortical state-space, we projected the articulator weightings for each electrode onto each principal component. This is possible because both PCA used to define the cortical state-space and the GLM analyses are linear descriptions of the recorded high-gamma activity. Articulator weightings correspond to a linear transformation of the articulator state into high-gamma activity, while the weightings of each electrode in each PC corresponds to a linear transformation of those electrode's high-Gamma activity into PC space. Across PC's, we found that the magnitude of the articulator weightings ($\log_{10}(|(PCNi*Wij)|)$) was significantly biased towards tongue over lips ($P < 0.05$) over jaw and larynx ($P < 0.001$ for each), while the difference between jaw and larynx was not significant ($P > 0.2$). This demonstrates that the structure of phonetic representations in the cortical state-space will be more heavily organized by the tongue and lips features than the jaw and larynx. This systematic bias in articulator weightings is in line with the organization of the cortical state-space described in the text, which is clustered according to the major oral articulators (i.e. tongue and lip). Statistical significance determined by Wilcoxon signed-rank test, n = 266 electrodes across subjects for each PC, with post-hoc bonferroni correction for m = 6 comparisons per PC.

b) Magnitude of articulator weightings in the 1st three PC's for the subjects individually. The rank-ordering of articulator weightings in PC's is a general feature of the individual subjects.

Supplementary Figure 10

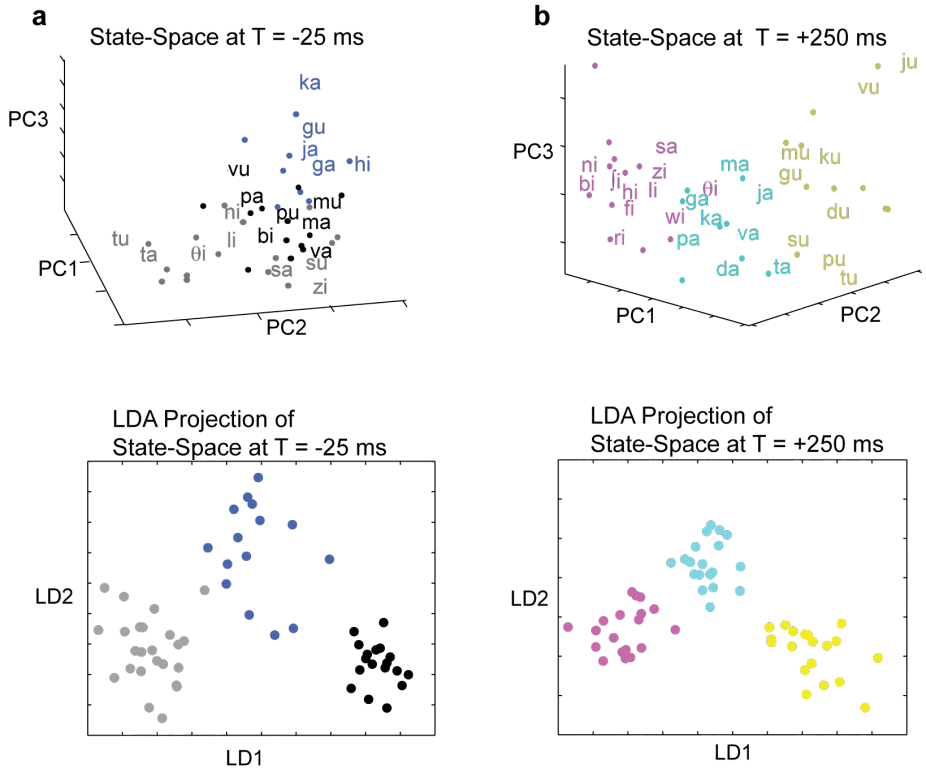

Supplementary Figure 10. Visualization of Linear Discriminate Analysis Projection of Cortical State-Space

We performed LDA on the 9 dimensional principle components space at the consonant and vowel time points, using the major oral articulators and vowel identity as labels (i.e. labial, dorsal tongue, coronal tongue for consonants and /a/, /i/, and /u/ for vowels, k = 3 clusters for both).

(top) Here we re-plot the cortical state-space defined by the first three principal components derived from the covariance matrix of the high-gamma z-scores at the consonant time (a) and at the vowel time (b). In this display, unsupervised k-means clustering was used to group syllables according to distances in the full nine-dimensional PC state-space.

(bottom) Projection of the cortical state-space onto the first two linear discriminate axes designed to accentuate the major oral articulator clusters (a) and the vowel clusters (b). The three major clusters are more separated in the LDA rotation than in the original, unsupervised PCA projection. This is to be expected as LDA explicitly looks for rotations of the axes that maximize the (linear) discriminability of these (experimentally defined) clusters.

We caution against detailed comparisons between the LDA projection and the cortical state-space dendrogram (Figure 5). The dendrogram is derived from the full distance structure of the 9-D cortical state-space, which is in turn derived from unsupervised PCA of the entire cortical data set. In contrast, the rotations of the PCA space found by LDA are designed to accentuate the three major clusters (experimentally defined), and are therefore likely to distort structure not put into the algorithm (e.g. constriction location and constriction degree).

Supplementary Figure 11

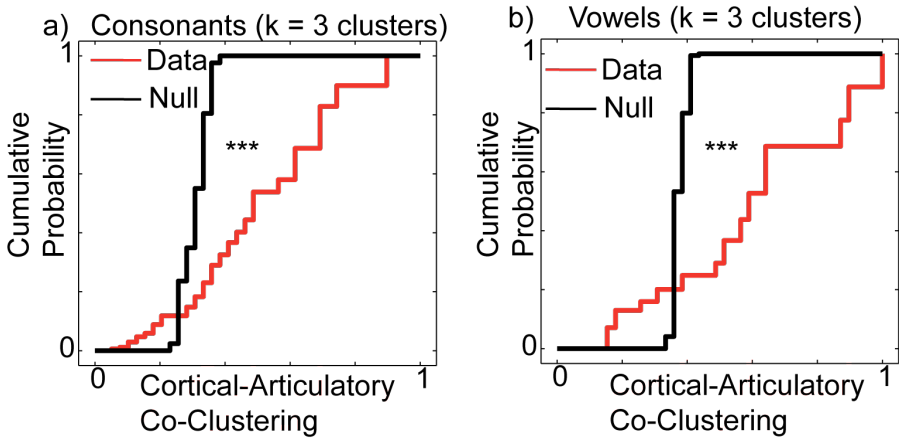

Supplementary Figure 11. Clustering of CVs in cortical state-space co-clusters with distinguishing articulator features for consonants and vowels.
To quantify the degree to which CVs were clustered in cortical state-space according to articulatory constraints, we calculated the co-clustering coefficient of CV syllables. The co-clustering coefficient quantifies the set theoretic overlap between two separate assignments of the same set of tokens to categories. Coefficients are one if and only if the two separate categorical assignments of tokens induce identical clusters of the tokens (100% overlap). Coefficients are zero if and only if every token clustering with a given token in one categorization is in a different cluster in the other categorization (0% overlap). See Methods for mathematical definition.

a) Cumulative distribution of co-clustering coefficients for each CV across subjects, Consonants. Here, we calculated the co-clustering coefficient for each CV when categorized by k-means (k = 3) clustering in the cortical state-space at a consonant time in each subject, and when categorized according to the three major articulators (Labial, Dorsal Tongue, Coronal Tongue). Across subjects, we found that clustering of CV's in the cortical state-space co-clustered with the major articulators significantly more than expected by chance (Red: observed distribution, median = 0.50, Black: null distribution from 1000 random permutations of articulator assignments of CVs, median = 0.32; ***: $P < 10^{-20}$, Wilcoxon signed-rank test, n = 168 syllables from three subjects). Similar results were obtained for each subject individually (Wilcoxon signed-rank test, $P < 10^{-6}$, bonferroni corrected for m = 3 comparisons, data not shown).

b) Cumulative distribution of co-clustering coefficients for each CV across subjects, Vowels. Here, we calculated the co-clustering coefficient for each CV when categorized by k-means (k = 3) clustering in the cortical state-space at a vowel time in each subject, and when categorized according to the three vowels (/a/, /i/, and /u/). Across subjects, we found that clustering of CV's in the cortical state-space co-clustered with the three vowels significantly more than expected by change (Red: observed distribution, median = 0.65; Black: null distribution, median = 0.37; $P < 10^{-15}$, Wilcoxon signed-rank test, n = 168 syllables from three subjects, not all subjects had all syllables). Similar results were obtained for each subject individually (Wilcoxon signed-rank test, $P < 0.05$, bonferroni corrected for m = 3 comparisons, data not shown).

Supplementary Figure 12

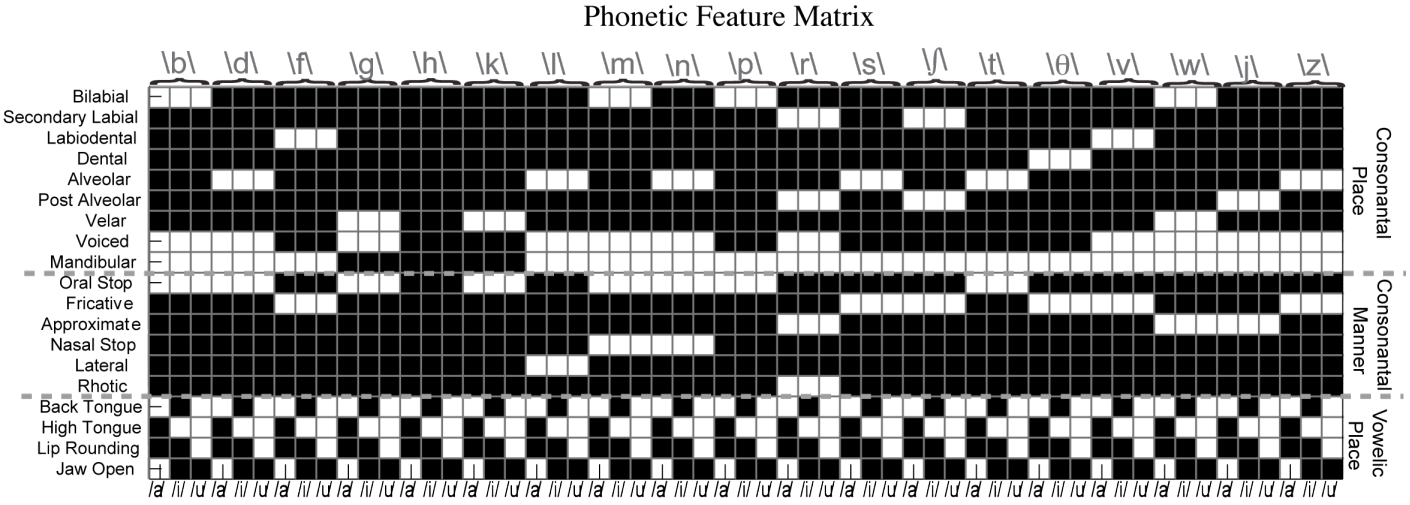

Supplementary Figure 12. Phonetic feature matrix.
For the analysis of phonetic structure of the CVs in our data set, we used a standard description derived from IPA. This feature matrix has nine features for the constriction location (~place of consonant articulation), six features for the constriction degree and shape (~manner of consonant articulation), as well as four features describing vocalic articulator configurations. IPA symbols for consonant (top) and vowel (bottom) segments are presented. White boxes correspond to 1, black to 0.

Supplementary Figure 13

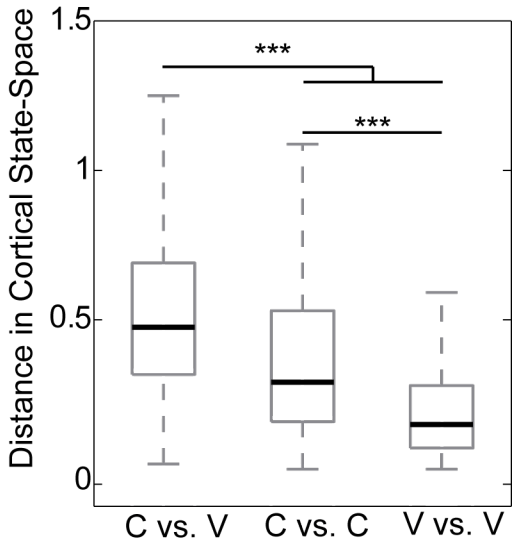

Supplementary Figure 13. Comparison of consonant and vowel representations
Here we display the distributions of distances comparing consonant and vowel representations. We found that the distribution of distances comparing consonants and vowels was significantly greater than the consonant-consonant comparison or vowel-vowel comparison, and the consonant-consonant comparison was greater than the vowel-vowel comparison ($P < 10^{-10}$ for all comparisons, Wilcoxon signed-rank test, n = 4623 for all, bonferroni corrected for m = 3 comparisons). Black line in plots correspond to median of data; grey boxes correspond to 25th and 75th percentiles, whiskers extend to ± ~2.7 s.d..

Supplementary Table 1. Clinical information

Here we present the clinical information regarding study subjects, and written explanation of grid placement. The first indication for placement of intracranial electrodes was for the localization of epileptogenic foci in patients in whom the seizure onsets were lateralized to one hemisphere using non-invasive workup. The second indication is to facilitate clinical electrical stimulation mapping (in dominant hemisphere) to define the localization of essential language sites prior to surgical excision. The decision for electrode placement was determined at an epilepsy surgery multidisciplinary case conference, and the decision is completely based upon clinical indications alone. In addition to the electrode array, other electrodes are placed to cover the subtemporal cortex (for fusiform and parahippocampal gyrus), frontal cortex (orbital frontal and dorsolateral prefrontal), and the parietal cortex, along with depth electrodes in the medial temporal structures (amygdala and hippocampus). Electrodes are routinely placed over peri-Sylvian cortex for pre-operative language mapping using electrical stimulation during counting and picture naming. The peri-Sylvian cortex includes Broca's and Wernicke's areas.

We do not suspect that epilepsy had an important effect on their articulatory processing. In each subject, the seizures were localized to areas outside of the ventral Rolandic cortex and had normal verbal fluency without indication of dysarthria or motor speech disorder in spontaneous speech and also our analysis of their speech syllable productions.

Supplementary Table 1

Subject ID	Grid Placement	Cerebral Language Dominance by Wada Testing	MRI	Seizure Focus Location	Speech Articulation	Postoperative Seizure Control
EC2	Left Perisylvian Cortex	Left	Normal	Posterior temporal cortex	Normal fluency, No dysarthria	Seizure-free
EC33	Right Perisylvian Cortex	Right	Normal	Hippocampus, Medial Temporal Lobe	Normal fluency, No dysarthria	Seizure-free
EC31	Left Perisylvian Cortex	Left	Normal	No seizures during prolonged hospitalization	Normal fluency, No dysarthria	Seizure-free*

* This patient did not have any seizures localized despite extensive monitoring and prolonged hospitalization (30 day implantation). Interestingly, postoperatively she did not experience any convulsive seizures for the two years of clinical follow-up so far, even though no resection was carried out. Similar observations have been made in the literature before, and it is thought that perioperative steroids, direct cortical manipulation, or other factors may affect the epileptogenic network.

Epilepsy control following intracranial monitoring without resection in young children. Roth J, Olasunkanmi A, Ma TS, Carlson C, Devinsky O, Harter DH, Weiner HL. Epilepsia. 2012 Feb;53(2):334-41.

Supplementary Methods

Spatial Cross-Correlation Analysis

We quantitatively analyzed the spatial organization of articulator representations using a two-dimensional cross-correlation analysis (Supplementary Figure 3). This quantifies the similarity of spatial structure of two matrices as they are 'slid' over each other at different spatial shifts in the x-direction (e.g. anterior-posterior direction) and the y-direction (e.g. dorsal-ventral direction). Generally speaking, two-dimensional cross-correlation analysis is capable of revealing important spatial characteristics, and has been utilized in the analysis of grid cells in entorhinal cortex[55]. In this paper, we use it primarily to examine two key features of the somatotopic map: 1) the consistency of spatial location of individual articulators across subjects, and 2) the consistency of the dorsal-ventral sequence of articulator representations within an individual. To gauge the significance of these analyses, we compared the results derived from analysis of observed data to a null data set created by randomly permuting the spatial location of selected electrodes prior to any analysis or processing. We first examined the structure of the with-in articulator, with-in subject autocorrelation. This provides information regarding the spatial contiguity of articulator representations, and any reproducible repeating structure (e.g. grid cells), or anisotropies (i.e. preferred angles of orientation). To address the consistency of the spatial location of individual articulators across subjects, we cross-correlated the maps for a single articulator across pair-wise comparisons of subjects (i.e. Lips in S1 vs. Lips in S2, etc). To address the consistency of the spatial ordering of articulators along the dorsal-ventral axis, we cross-correlated neighboring articulator representations across pair-wise sequential comparisons (i.e. Larynx vs. Tongue, Tonuge vs. Jaw, Jaw vs. Lips) within a subject. The results of these analyses, presented in Supplementary Figure 3, demonstrate that the key features of the summary articulator maps are statistically reproduced in individual subjects.

Spatial Organization Analysis

To further understand the observed functional organization of articulator representations, we measured the average Euclidean distance (in mm) between electrodes categorized according to their preferred articulator (winner-take-all categorization). We compared the distributions of average intra-articulator distances and cross-articulator distances to predictions from a perfect linear somatotopy and from a completely random scattering (1000 maps each, see Methods). These null models had similar parameters to the observed organization (same number of points per articulator, approximately the same range of spatial values and total area covered) and were used as bounding conditions to set the scale for possible outcomes (Supplementary Figure 5).

Co-clustering Coefficient

The co-clustering coefficient (Supplemental Figure 7) is defined over a set of n tokens and describes the degree of overlap between cluster memberships when these tokens are separated into clusters in different ways (e.g. clustered in different spaces). Each CV

syllable, s_i, can be clustered in both the cortical state-space and according to the major oral articulators. This clustering will give rise to an assignment of s_i to cortical cluster j (NC_j) and articulator cluster k (AC_k), where NC_j and AC_k are the sets of syllable assignments to cortical cluster j and articulator cluster k, respectively, and can be of different sizes ($|NC_j| \neq |AC_k|$). Here, we have defined the articulator clusters according to the known major articulator for the consonants, and according to vowel identity for vowels. For each s_i, the associated co-clustering coefficient, $\kappa(s_i) \in [0\ 1]$, is defined in terms of the normalized, symmetric set theoretic difference between $NC = NC_j \backslash s_i$ (i.e. the syllables in NC_j other than s_i) and $AC = AC_k \backslash s_i$:

(1) $$\kappa(s_i) = 1 - \frac{|NC \Delta AC|}{|NC| + |AC|}$$

Where Δ is the symmetric difference operator: for two sets A and B, $A \Delta B = (A \backslash B) \cup (B \backslash A)$.

$\kappa(s_i)$ takes the value 1 if every syllable that is in the same cluster as s_i defined in one space is also in the same cluster as s_i defined in the other space (e.g. NC = AC). Conversely, $\kappa(s_i)$ takes the value 0 if every syllable that is in the same cluster as s_i defined in one space is in a different cluster than s_i defined in the other space (e.g. $NC \cap AC = 0$).

We estimated the expected value of $\kappa(s_i)$ under the null hypothesis of no relationship between clustering in cortical state-space and clustering according to major articulator by randomly permuting cluster identity according to articulator while leaving the clustering in the cortical state-space unchanged. This procedure was repeated independently 1000 times for every CV syllable for each subject, and the average of the repetitions was used as the estimate of $\kappa(s_i)$ under the null hypothesis.

LDA projection of cortical state-space

Multiclass LDA was performed on the cortical state-space representations (**K**) at consonant and vowel times by computing the matrix $\mathbf{A}^* = \mathbf{A}\mathbf{B}^{-1/2}$, where **A** and **B** are the class centroids and common with-in class covariance matrices, respectively. Syllables were classified according to major oral articulators (labial, coronal, dorsal) for consonant times and the three vowels (/a/, /i/, and /u/) for vowel times. We then performed SVD on the covariance matrix of $\mathbf{A}^*$, and projected the state-space representations of syllables into the first two dimensions of the corresponding eigenspace.

55. Hafting, T., *et al*. (2005) Microstructure of a spatial map in the entorhinal cortex. *Nature* 436, 801-806